Interatomic scattering in energy dependent photoelectron spectra of Ar clusters

M. Patanen, S. Benkoula, C. Nicolas, A. Goel, E. Antonsson, J. J. Neville, and C. Miron

Citation: The Journal of Chemical Physics **143**, 124306 (2015); doi: 10.1063/1.4931644
View online: http://dx.doi.org/10.1063/1.4931644
View Table of Contents: http://scitation.aip.org/content/aip/journal/jcp/143/12?ver=pdfcov
Published by the AIP Publishing

Interatomic scattering in energy dependent photoelectron spectra of Ar clusters

M. Patanen,[1] S. Benkoula,[1] C. Nicolas,[1] A. Goel,[1,a)] E. Antonsson,[1,2] J. J. Neville,[1,3] and C. Miron[1,4,b)]

[1]*Synchrotron SOLEIL, L'Orme des Merisiers, Saint-Aubin, BP 48, 91192 Gif-sur-Yvette Cedex, France*
[2]*Physikalische und Theoretische Chemie Institut für Chemie und Biochemie, Fachbereich Biologie, Chemie, Pharmazie, Freie Universität Berlin, Takustrasse 3, 14195 Berlin, Germany*
[3]*Department of Chemistry, University of New Brunswick, Fredericton, New Brunswick E3B 6E2, Canada*
[4]*Extreme Light Infrastructure - Nuclear Physics (ELI-NP), 'Horia Hulubei' National Institute for Physics and Nuclear Engineering, 30 Reactorului Street, RO-077125 Măgurele, Jud. Ilfov, Romania*

(Received 11 June 2015; accepted 11 September 2015; published online 28 September 2015)

Soft X-ray photoelectron spectra of Ar 2p levels of atomic argon and argon clusters are recorded over an extended range of photon energies. The Ar 2p intensity ratios between atomic argon and clusters' surface and bulk components reveal oscillations similar to photoelectron extended X-ray absorption fine structure signal (PEXAFS). We demonstrate here that this technique allows us to analyze separately the PEXAFS signals from surface and bulk sites of free-standing, neutral clusters, revealing a bond contraction at the surface. © *2015 AIP Publishing LLC*. [http://dx.doi.org/10.1063/1.4931644]

I. INTRODUCTION

The surface properties of clusters and nanoparticles and their chemical reactivity are of fundamental relevance to a large variety of research fields. For example, the role of surface chemistry of nano-objects is of utmost importance in catalysis and its industrial applications, as well as in nature.[1,2] The unique surface properties of nanomaterials can be used to enhance materials' properties in energy conversion and energy storage technologies.[3] Photoelectron diffraction and photoelectron scattering have been shown to be powerful techniques to study surfaces and adsorbates due to their pronounced surface sensitivity.[4] In an (Extended) X-ray Absorption Fine Structure ((E)XAFS) measurement, the absorption by the sample of monochromatic X-rays from a tunable source, such as synchrotron radiation, is monitored either directly, by recording the amount of attenuation of the X-ray beam, or indirectly, by collecting a yield of secondary particles (electrons, photons, ions) generated by the relaxation of the excited state created by the absorption of X-rays. In the vicinity of a core level, below the ionization threshold an increase is observed in the absorption when the energy of the X-rays matches exactly the energy needed to promote a core-electron to an unoccupied electronic state. Above the ionization threshold a photoelectron is emitted, which can, in a simplified picture, be modeled by a spherical wave propagating in the material and being scattered by the neighbors of the emitting atom. The neighboring atoms serve as point sources for backscattered waves, and when the outgoing and backscattered electron waves interfere constructively, the recorded absorption signal is enhanced. Similarly, when destructive interference occurs, a decrease of the absorption signal is observed. A key parameter is the phase of the backscattered electron wave, which depends on the spatial distance between the photoelectron emitter and the scatterer, and thus the oscillatory interference pattern observed in the absorption signal provides structural information about the studied sample. In X-ray photoelectron spectroscopy (XPS), X-rays are used to ionize the sample and the kinetic energies of the emitted photoelectrons are analyzed. Since photoelectron spectroscopy is very sensitive to the chemical environment (at both intra- and intermolecular levels), shifts in photoelectron binding energies give an additional, chemical-state specificity. EXAFS and XPS techniques can be combined in a technique called photoelectron EXAFS (PEXAFS), where the electrons emitted from the sample when scanning X-ray energy are also energy analyzed.[5] Sieger *et al.*[6] showed that instead of recording an absolute PEXAFS signal, the same information can be derived from the branching ratio of two spin-orbit-split peaks of a given core level. They recorded the Sb 4d level with spin-orbit splitting of 1 eV from Sb/Si(111) $\sqrt{3}\times\sqrt{3}$ and $5\sqrt{3}\times5\sqrt{3}$ absorbates, and they were able to differentiate these absorbate structures by EXAFS analysis based on the measured branching ratios. They pointed out that this intensity ratio method involving two peaks with nearly the same energy can be more accurate than absolute intensity measurements, since several normalization issues are divided out.

A very similar technique is the chemical shift photoelectron diffraction (CSPD), which has been utilized to reveal, for example, different orientations of adsorbates containing the same elements.[7,8] PEXAFS-type measurements have been carried out for isolated, gas-phase molecules as well (see, e.g., Ref. 9 and references therein), and for further discussion of the differences and similarities of electron scattering and diffraction measurements, the reader is referred to a recent review by Mårtensson *et al.*[10]

Argon clusters have represented a showcase example for soft X-ray spectroscopy for over 20 years. Rühl and coworkers[11,12] have measured total ion yields (TIY) of Ar

a)Laboratory of Surface Science and Technology, Department of Materials, ETH Zürich, HCI G543, Zürich CH-8093, Switzerland.
b)Electronic mail: Catalin.Miron@synchrotron-soleil.fr

clusters and found that the (EXAFS) signal is very similar to that of solid Ar, but there are larger contributions of disorder effects and thermal motion (vibrations), seen as an increased Debye-Waller factor, i.e., attenuation of the absorption signal. Björneholm *et al.* presented both Ar 2p absorption and photoelectron spectra of Ar clusters of different sizes and, owing to the chemical shift of the surface states, they were able to obtain information about the effective coordination numbers of surface atoms.[13] After these pioneering studies, numerous other fundamental properties of rare gas clusters have been demonstrated at the Ar 2p edge of Ar clusters, including angular distributions,[14] fragmentation,[15] inter-atomic Coulombic decay (ICD),[16] and photoelectron recapture.[17] In the present work, we demonstrate the applicability of the PEXAFS-type of measurements to study unsupported clusters, by recording the 2p photoelectron spectrum of Ar clusters over an extended energy range. The method can be used in the electron kinetic energy range ≈2–6 $Å^{-1}$, allowing us to perform an X-ray absorption spectrum (XAS) analysis determining the nearest neighbor distances independently for both surface and bulk sites. The results are in line with the EXAFS study of Ar clusters by Rühl *et al.*,[11,12] but compared to total yield measurements, our energy selected photoemission directly referenced to an atomic cross-section has certain benefits: surface and bulk can be studied independently, the measurement is not disturbed by the opening of new photoionization channels, and some normalization issues are avoided. As limitations of the method, we would mention a sensitivity to the experimental conditions, and due to the transmission properties of the hemispherical electron analyzer, the very low kinetic energies which are probing the multiple scattering regime are not accessible.

II. EXPERIMENT

The experiment was carried out at the PLEIADES beamline[18,19] at the SOLEIL national synchrotron radiation facility in Saint-Aubin, France. The Apple II permanent magnet HU80 (80 mm period) undulator was used to provide linearly polarized light with 54.7° between the polarization vector and the electron detection axis. The Ar 2p photolines were recorded using a 30° wide-angle lens VG-Scienta R4000 electron energy analyzer installed on the C-branch of the beamline. The analyser's electron detection axis is perpendicular to the storage-ring plane, and it is mounted perpendicular to the propagation direction of the ionizing radiation, i.e., in the so-called dipole plane. The photoionization asymmetry parameter β of Ar 2p varies between 0.6 and 1.4 in the kinetic energy range studied here, and we selected a "magic angle" between the polarization vector of the light and the detection axis of the electron analyzer, to ensure that the cross-section is independent of the angular anisotropy. It is known that the elastic scattering makes photoelectron angular distributions more isotropic in case of randomly oriented clusters.[20] However, in our experiment, the choice of the analysis angle in the laboratory frame makes our experiment asymmetry independent. Furthermore, the randomly oriented sample singles out the effect of the elastic scattering modifying the angular distributions, in contrast to X-ray photoelectron diffraction experiments of well oriented samples. The degree of linear polarization of the photon beam is better than 98%.

The setup used for in-vacuum cluster generation is described elsewhere.[21] In short, the clusters were produced from Ar gas of 99.998% stated purity (Air Liquide) via adiabatic expansion through a liquid nitrogen cooled nozzle (100 μm). The temperature of the nozzle was kept constant (117 ± 0.5 K) and different cluster sizes were produced by varying the backing pressure between 0.7 and 2 bar. The size estimation derived from these experimental parameters is based on the well-known scaling law proposed by Hagena,[22] and the formula used here for large clusters is presented in Ref. 23 based on the study by Karnbach *et al.*[24] We get $\langle N \rangle$ = 400, 1600, and 3000 as the estimates for the mean sizes, but a detailed lineshape analysis of Ar 2p photoionization spectra carried out by Bergersen *et al.*[25] indicates that these sizes are underestimated. It is important to point out that like many nanosized systems produced by growth in vapor phase, the size distribution of the cluster beams is found to have a lognormal distribution[26,27] with Full Width at Half Maximum (FWHM) as large as $\langle N \rangle/2$.[25]

The instrumental broadening was kept at 130 meV over the entire energy range (273–420 eV) by adjusting the monochromator exit slit while keeping the settings of the electron analyser constant (pass energy of 50 eV and curved entrance slit of 0.8 mm). At photon energies 263–271 eV (low kinetic energies), a pass energy of 10 eV was used to minimize the effect of the rapidly changing transmission function at kinetic energies below the pass energy. Our electron energy analyzer has a typical exponential transmission function and the low kinetic energy spectra were corrected using a method described by Jauhiainen *et al.*[28] based on the assumption of a constant ratio of the intensities of the Xe 4d photolines and $N_{4,5}OO$ Auger lines at all photon energies. The total experimental broadening was around 80 meV in these low pass energy measurements, the major contribution coming from the photon bandwidth. A varied groove depth (VGD) plane grating with 600 grooves/mm was used. In the fits, we used the lifetime broadening of the Ar 2p lines reported to be 119 meV.[29]

In order to avoid normalization issues, instead of trying to extract absolute cross sections/XAS signal, we studied relative cluster-to-atom cross sections. As in an example spectrum presented in Fig. 1, at each photon energy the photoelectron spectrum consists of atom, cluster-surface, and cluster-bulk

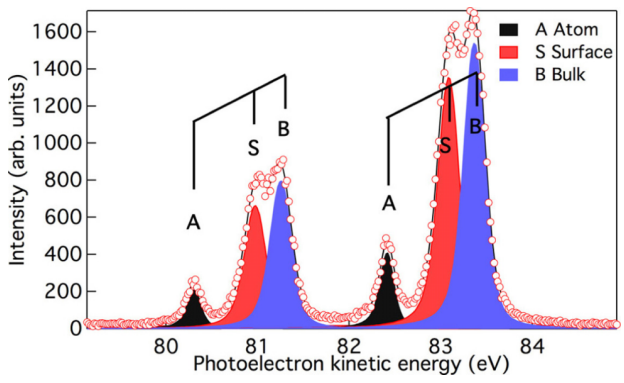

FIG. 1. An example of the experimental Ar 2p XPS spectrum of clusters with an average size of 400 atoms.

components, whose intensity ratios are studied. Assuming that the number of free and condensed atoms remains constant, the data do not require normalization in terms of experimental parameters. Some sample dependent normalization is, nevertheless, further needed due to the changing electron attenuation length which will be discussed below. However, this means that very stable experimental conditions are essential for this experiment. The backing pressure, the pressure in the experimental chamber, and the temperature of the nozzle were constantly monitored, and the data where their values changed were disregarded. Stable conditions were also verified by recording the same spectrum at certain photon energies from time to time, and checking that the bulk-to-surface ratio remained constant. The data obtained for the smallest cluster size are of the best quality in terms of conditions' stability. In the case of the largest size, the nozzle started to freeze and thus also the error bars of the ratios are larger.

III. DATA ANALYSIS

Ar 2p photolines were fitted using Igor Pro software by WaveMetrics, Inc. and the SPANCF fitting macros by Kukk.[30–32] An example of the fit is shown in Fig. 1. For a given set of conditions (given mean cluster size), the relative energy separation was kept constant as well as the Lorentzian broadening corresponding to the lifetime of the Ar 2p core vacancy. An asymmetric lineshape was used in order to take into account the tail towards lower kinetic energies due to the post-collisional interaction (PCI).[33] Thanks to well separated Ar $2p_{1/2}$ and $2p_{3/2}$ spin-orbit (s-o) components (s-o splitting of 2.2 eV), from each spectrum we obtained 6 intensity ratios: surface-to-atom, bulk-to-atom, and bulk-to-surface ratios of both s-o components. It can be assumed that over 10 eV above the ionization threshold, there is no significant difference between the cross sections of the two s-o components and thus, from now on, we speak about the "non-relativistic" Ar 2p relative cross sections. Consequently, at a given photon energy, from each spectrum we obtained two experimental intensity ratios with two kinetic energies for a given data set (surface-to-atom, bulk-to-atom, and bulk-to-surface). The 2p ionization of Ar clusters serves as a good proof-of-principle, because more than 10 eV above threshold the atomic photoionization cross section is a monotonic function free from Cooper minima, which would possibly complicate the analysis based on relative cross sections between cluster sites (surface and bulk signals) and the atomic signal.

The experimental intensity ratios were further analysed using Athena software[34] in order to perform a Fourier transform to obtain the nearest neighbor distances. All the data were analyzed using the same Hanning window from 2 to 6 Å and using the phase correction option (based on calculated phase shifts) of the Athena software. The phase shift was found to shift the nearest neighbor distances by ≈0.2 Å towards higher values.

IV. CALCULATIONS

Model calculations were carried out using the real-space multiple-scattering code FEFF9[35] in order to show that the observed oscillations in the cluster-to-atom ratios are in qualitative agreement with the XAS signal modulated by electron scattering. Calculations were performed for a face-centered cubic (fcc) structure with N = 459, which is known to be the structure of solid Ar with a lattice constant of 5.26 Å.[36] Other structures and sizes were tried, as, for example, the icosahedral structure with the same nearest neighbor distance, but it was found that in the energy region of our experimental data, the fcc fits the data the best, while the differences between the different structures are very small. The low energy part (multiple scattering regime) is much more sensitive to the crystal structure, but unfortunately the experimental method used here is not applicable to this region. Even if the absorption signal $\chi_i = \mu_i/\mu_{0i} - 1$, where μ_i is the cluster absorption and μ_{0i} is the atomic background absorption (calculated in the dipole approximation), gives readily qualitatively comparable signal to the experimental ratio, the absolute ratios cannot be compared since the absolute number of gas phase atoms versus number of atoms condensed to clusters is unknown.

There are many inequivalent surface atoms in the cluster (edge, face, corner/vertex), but the chemical shifts between these components are smaller than the Ar 2p lifetime broadening and we are not able to separate them in the photoelectron spectrum. The cluster sizes studied here (400, 1600, 3000) are relatively large, and even for the smallest size the surface atoms are mostly sitting on the edge or face of the cluster, less coordinated corner/vertex atoms being a much smaller contribution. When modeling the χ_i signal it was noticed that in the studied energy range the main difference between the face and the edge components is only in the amplitude of the oscillation, edge atoms having fewer neighbors and thus smaller amplitude. Thus, we selected to show in the following, Figs. 2 and 3, the simulation with a face atom as an absorbing atom. In our calculations, the Debye-Waller temperature was kept at 89 K.[37]

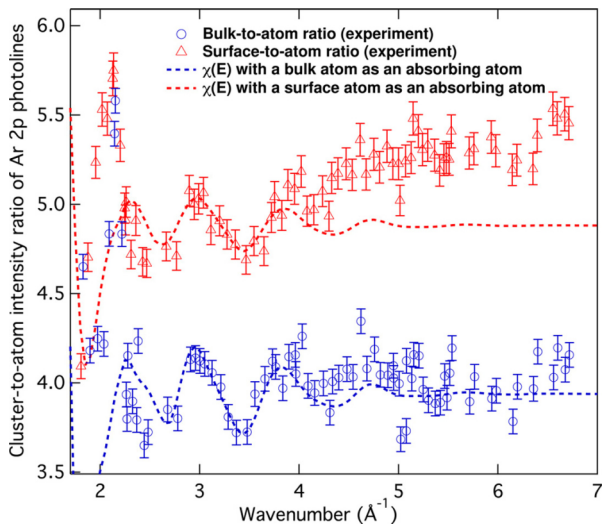

FIG. 2. Surface-to-atom (red triangles) and bulk-to-atom (blue circles) Ar 2p intensity ratios of clusters with an average size of 400 atoms as a function of photoelectron kinetic energy compared to model calculations for the fcc-crystal structure. Error bars in the determination of the cross section ratios are also shown. The simulated χ curves have been vertically aligned for better visual comparison since the absolute absorption cross sections cannot be determined from the experiment, but they are not shifted in energy.

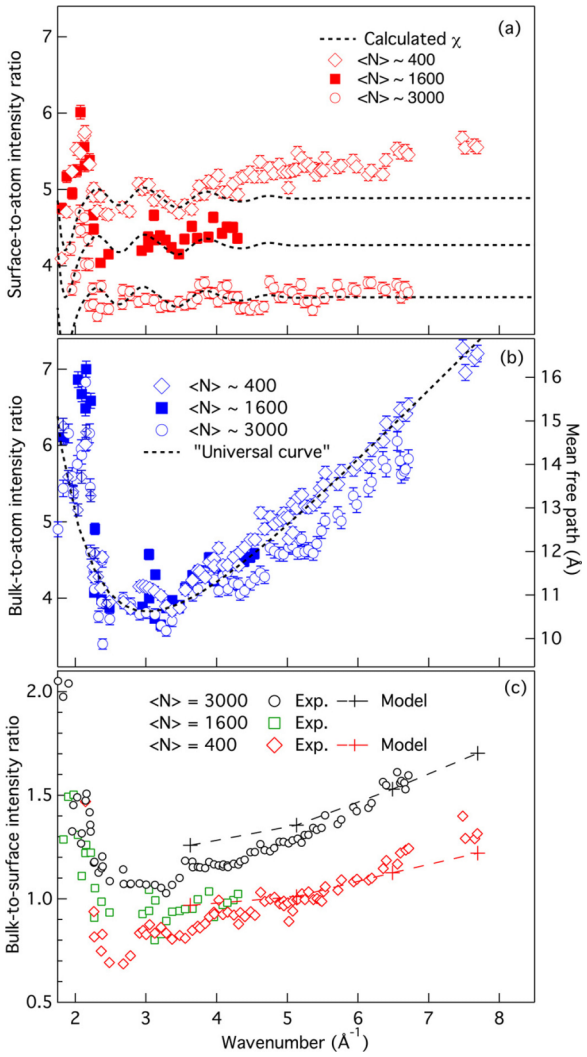

FIG. 3. (a) A comparison between surface-to-atom ratios and (b) bulk-to-atom ratios of Ar clusters with different sizes: ⟨N⟩ = 400, diamonds; ⟨N⟩ = 1600, filled squares; ⟨N⟩ = 3000, circles. (c) Experimental bulk-to-surface intensity ratios compared to the ratio obtained from a simple model based on electron attenuation in a uniform sphere.

V. RESULTS AND DISCUSSION

Figure 2 presents the obtained Ar 2p surface-to-atom and bulk-to-atom intensity ratios and compares them to the model calculations of the XAS signal. The main result of this paper is the observation of the well-resolved oscillation with approximately the same oscillatory period in both surface-to-atom and bulk-to-atom intensity ratios between 2.5 and 4 Å^{-1}. The bulk-to-atom data present larger amplitude oscillation, which is reproduced by the calculation and can be reasoned by the different number of neighbors (point scatterers) around bulk and surface atoms. The oscillatory behavior observed is in agreement with the EXAFS study of Ar clusters by Rühl *et al.*[11,12] They could not measure the absorption signal above 4.5 Å^{-1} due to the opening of the 2s channel. This is, in principle, not a limitation for our method, and we were able to use data up to 6 Å^{-1} in the EXAFS analysis. Above that the oscillations are damped too much due to disorder effects like vibrations and imperfections. The bulk-to-atom intensity ratio is corrected by subtracting a fitted "universal curve"[38] representing a modulation bulk signal due to the electrons' escape depth from the clusters.

The low energy part, below 2.5 Å^{-1}, starts to deviate significantly from the simulation for many reasons, but the bulk-to-atom intensity ratio at low kinetic energies is particularly distorted compared to the simulation. This is partly due to the difficulties to fit the universal curve to the oscillating signal: very likely there is a maximum around 2 Å^{-1} but it is either overestimated in the experiment as discussed below or underestimated by the calculation due to the fact that the increase in the escape depth is not properly taken into account in the calculation. The surface-to-atom ratio of the smallest size clusters displays a monotonic increase at large kinetic energies. Since this is observed only with the smallest size clusters, we assumed that the origin of this effect is the increased mean free path of electrons: at higher kinetic energies (similarly, at very low kinetic energies) we effectively "see" more surface atoms, i.e., photoelectrons which are attenuated inside the cluster at lower energies can now reach the detector. This assumption is further confirmed by modeling as described below. Furthermore, since the atomic cross section to which the data are referenced is changing rapidly at low kinetic energies, the method to extract the intensity ratios becomes less reliable. The chemical shift between the atomic and surface (bulk) component is 0.64 eV (0.92 eV) for ⟨N⟩ = 400 average size, and when taking the intensity ratios, the cluster component is normalized by a lower kinetic energy atomic component, and the data are presented with respect to the kinetic energy of the photoelectron emitted from the cluster. This effect was corrected by using the calculated atomic cross section[39] and scaling the measured atomic intensity with the atomic cross section ratio between the cross section at the measured kinetic energy of the atom and at the kinetic energy of the cluster peak. This turned out to be a rather small correction, but on the other hand it is strictly based on calculated cross sections. If the maximum of the atomic cross section is shifted in reality, this can drastically influence the cluster-to-atom ratios at low energies.

Additionally, the PCI effect is very strong at low kinetic energies and makes the fitting procedure challenging, combined also with an increased background due to the tail of zero kinetic energy electrons, which is rather intense due to the increase in the transmission of the hemispherical analyser. Thus, the experimental method used here is not optimal for the low kinetic energy region, where another type of electron energy analyzer like a time-of-flight or velocity map imaging spectrometer should be used instead. This energy region, dominated by multiple scattering, would be beneficial when comparing the signals from different crystal structures, for example, as there have been indications that the Ar clusters have icosahedral structures when the size is about a few hundreds of atoms, and fcc structures for larger sizes.[40] Recently, also a possible fcc-to-hcp transition has been reported for cluster sizes much larger than those used in our study.[41] The electron kinetic energy region where our technique performs well is mostly probing the single scattering events with nearest neighbors, and model calculations did not show sensitivity to the structure in this range.

Figure 3(a) shows a comparison between surface-to-atom ratios for different cluster sizes, and Fig. 3(b) compares the

bulk-to-atom ratios. The smallest size data show the oscillations best (presented also in Fig. 2), but the two other sizes behave rather similarly. Noteworthy, the surface-to-atom ratio of the largest size seems to stay constant at higher energies, in contrast to the smallest size, indicating that these clusters are so large that emitted electrons cannot penetrate the whole cluster.

All bulk-to-atom ratios are rather similar, exhibiting the shape of the "universal curve," with a minimum around 25 eV kinetic energy. This shape hides the oscillations and a single maximum around 3 $Å^{-1}$ is clear. The discontinuity in the experimental points of $\langle N \rangle = 400$ size around 7.2 $Å^{-1}$ is due to the region where the Auger electron lines overlap with the photoelectron lines. The inelastic mean free path for Ar can be estimated using the QUASES-IMFP-TPP-2M software[42] based on a TPP-2M predictive formula.[43] Using these attenuation lengths, we have performed a simple modelling for the probability of a given electron to reach the detector when it is originates from a certain atom at radius r from the center of the cluster. If the point was situated at further than one shell distance from the circumference, it was taken as an electron originating from a bulk atom, otherwise it was counted as an electron from a surface atom. The model assumes that the photon attenuation can be neglected and the whole cluster of radius R is described as a completely spherical uniform medium. The total cluster bulk and surface signals are obtained by integrating over all the angles with corresponding ranges of r. The ratios of probabilities for electrons originating from bulk and surface atoms were calculated for kinetic energies 50, 100, 160, and 225 eV (3.6, 5.1, 6.5, and 7.7 $Å^{-1}$) and for clusters with radii 1.75 nm and 2.7 nm as models of small and big clusters, respectively. The modeled ratios are found to be in good agreement with our experimental ratios presented in Figure 3(c), and indicating that the attenuation lengths obtained with QUASES-TPP-2M are realistic. Details of our simulations are presented in the supplementary material.[44] Noteworthy, the simulations show that for the smallest size, there is a non-zero probability for an electron emitted from the surface atom situated on the opposite side of the cluster related to the detector, to reach the detector. This confirms the idea that the monotonic increase of the surface signal (Fig. 3(a)) observed only in case of smallest clusters originates indeed from the fact that the attenuation length is long enough to detect photoemission signal from these opposite site surface atoms.

Tchaplyguine *et al.* have determined the electron escape depths for several rare gas clusters produced by adiabatic expansion using simulations and experimental data of mean sizes $\langle N \rangle = 300$ and 1000.[45] We find both our simulated and experimental bulk-to-surface ratios larger than their values for $\langle N \rangle = 300$, and they deduce a smaller (9 Å) electron escape depth for 50 eV kinetic energy compared to our value of 11 Å. Even though, in principle, this method based on surface-to-bulk intensity ratios can be very useful when determining the escape depths of electrons, in case of clusters created via adiabatic expansion, the accuracy is compromised due to the large size distribution of clusters. Size-selection or narrowing the size distribution would be beneficial.

Finally, Fig. 4 presents a comparison of magnitudes of the Fourier transform for the smallest and the largest size clusters, made from PEXAFS data obtained from cluster-to-atom ratio presented in Figs. 3(a) and 3(b) by subtracting a linear background in order to bring the oscillations of the data around 0. The data were not k-weighted before the Fourier transform. The bulk signal in Fig. 4(a) resembles the one obtained by Rühl *et al.* from K shell TIY of same average size Ar clusters.[12] The nearest neighbor distances for the smallest size are 3.72 ± 0.05 Å and 3.79 ± 0.05 Å, for surface and bulk components, respectively. We used a Gaussian fit to define the maximum of the peaks and the error bars represent the sensitivity of the maxima to small changes in the Hanning window. These data indicate a small surface bond contraction, order of 2%. Bond contraction of approximately same magnitude has been reported in deposited nanostructures using a different technique, and it was observed that this relaxation depends on coordination.[46] The surface exhibits much broader and somewhat structured first peak compared to the bulk peak, which is indeed expected taking into account that the surface component contains a signal from edge, corner, face, and defect atoms, which all can have different bond contractions. The second peak observed is stronger in surface signal and situated at 5.31 ± 0.05 Å and 5.46 ± 0.05 Å, for surface and bulk components, respectively. This value is close to the lattice parameter 5.26 Å of solid Ar.[36] The peak at 6.2 Å in solid Ar, corresponding to the fourth coordination shell,[12] is present in bulk (at 6.39 ± 0.05 Å) but almost absent in surface

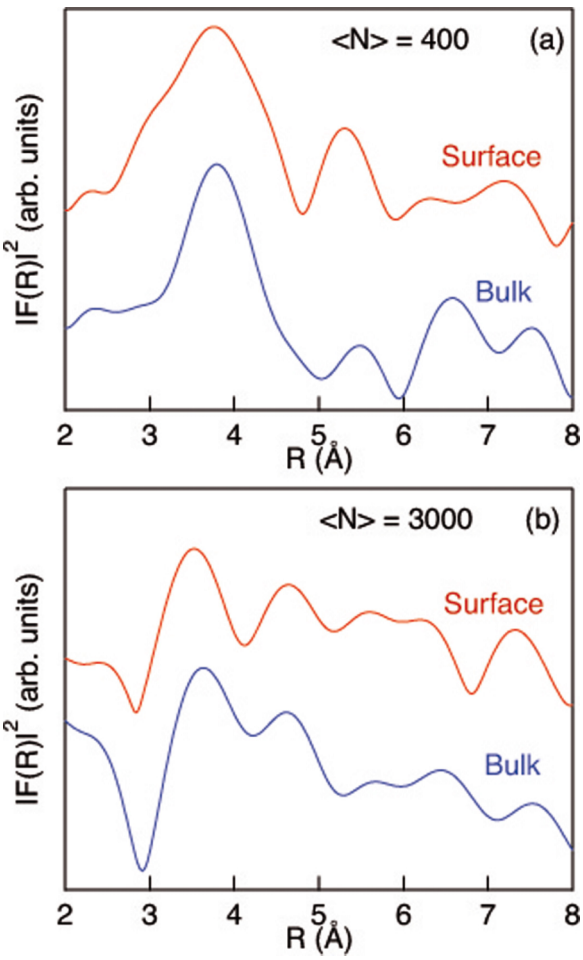

FIG. 4. Magnitude of the Fourier transform of the PEXAFS data for clusters with mean size (a) $\langle N \rangle = 400$, (b) $\langle N \rangle = 3000$.

(small peak at 6.16 ± 0.05 Å). The data for the largest size presented in Fig. 4(b) exhibit more structures, but the shape is similar for both surface and bulk. This is also an important indication that the "universal curve" background subtraction does not affect the signal too much, since for surface signal only a linear background was subtracted. The nearest neighbor distances are 3.53 ± 0.05 Å and 3.66 ± 0.05 Å, for surface and bulk components, respectively, so again the surface component is at smaller distances and slightly broader than the bulk. Similar to the case of smallest size, the backscattering peak around 6.4 Å in bulk is suppressed in surface signal. Both the surface and bulk signals show extra components compared to the smallest size, which can be interpreted so that the beam consists of two (or several) structures, e.g., fcc structure and another orthorhombic structure where all the atomic distances are not equal. Indeed, orthorhombic structures were observed and modeled in the work of Krainyukova *et al.*[41] The quality of our experimental data for the largest size is, however, not as good as for the smaller size, and apart from the clear peaks at first shell distances, interpretation of the other structures remains tentative.

We chose to study cluster-to-atom ratios instead of the spin-orbit ratios like Sieger *et al.*,[6] since the cluster-to-atom signal is directly proportional to the χ signal, whereas the method based on spin-orbit ratios is a differential method and would work the better the smaller the energy difference between the components is. Spin-orbit ratios have the benefit that the "universal curve" behavior of the bulk signal would be divided out, but it also requires further manipulation of the data, e.g., integration, and would reduce our data points by a factor of 2. For the smallest size clusters, we checked the first shell distances obtained from magnitudes of the Fourier transform of the PEXAFS data analyzed by the method introduced by Sieger *et al.*, and obtained 3.72(5) Å and 3.71(5) Å for surface and bulk, respectively. The values are very close to the values obtained from our direct cluster-to-atom ratio analysis. However, the peaks are broader and there is significantly larger contribution in very small radial distances. This completely independent method thus supports the first radial distances found, but also suggests that our experimental data are not sufficiently smooth for the integration steps needed in this method, or the spin-orbit energy splitting is too large (2.2 eV) so that this differential method is not applicable in the present case.

VI. CONCLUSIONS

We have carried out a photoelectron EXAFS experiment for Ar 2p levels of argon clusters. Cluster-to-atom intensity ratios exhibit periodic oscillations which were found to be in qualitative agreement with FEFF9 simulation of $\chi(E)$ EXAFS signal. The EXAFS analyses were carried out using ATHENA software revealing approximately 2%-4% nearest neighbor distance contraction on surface layer of Ar clusters of two different sizes. Our experimental bulk-to-surface intensity ratios agree well with the ones obtained by a simple modelling using inelastic mean free paths based TPP-2M model. Despite some of the difficulties to access the very low kinetic energy region with the current instrumentation, we have demonstrated that the photoelectron EXAFS method is applicable to free-flying, unsupported clusters, and it can be a powerful technique allowing to record EXAFS-signal from the same element but from different chemical environments.

ACKNOWLEDGMENTS

The experiment was performed at the PLEIADES beamline at the SOLEIL Synchrotron, France (Proposal No. 20131030). We thank E. Robert for technical assistance, and the SOLEIL staff for stable operation of the equipment and storage ring during the experiments. We want to thank Professor J. J. Rehr, Dr. J. Kas, and Dr. K. Gilmore for the discussions concerning the FEFF calculations, Dr. F. Sirotti for useful discussions concerning the mean free paths, and Dr. N. Trcera for introducing the Athena software to us.

[1]B. R. Cuenya, Thin Solid Films **518**, 3127 (2010).
[2]H. Häkkinen, Nat. Chem. **4**, 443 (2012).
[3]L. Dai, D. W. Chang, J.-B. Baek, and W. Lu, Small **8**, 1130 (2012).
[4]D. Woodruff, Surf. Sci. Rep. **62**, 1 (2007).
[5]G. M. Rothberg, K. M. Choudhary, M. L. denBoer, G. P. Williams, M. H. Hecht, and I. Lindau, Phys. Rev. Lett. **53**, 1183 (1984).
[6]M. T. Sieger, T. Miller, and T.-C. Chiang, Phys. Rev. Lett. **75**, 2043 (1995).
[7]R. L. Toomes, R. Lindsay, P. Baumgärtel, R. Terborg, J.-T. Hoeft, A. Koebbel, O. Schaff, M. Polcik, J. Robinson, D. P. Woodruff, A. M. Bradshaw, and R. M. Lambert, J. Chem. Phys. **112**, 7591 (2000).
[8]K.-U. Weiss, R. Dippel, K.-M. Schindler, P. Gardner, V. Fritzsche, A. M. Bradshaw, D. P. Woodruff, M. C. Asensio, and A. R. Gonzalez-Elipe, Phys. Rev. Lett. **71**, 581 (1993).
[9]J. Söderström, N. Mårtensson, O. Travnikova, M. Patanen, C. Miron, L. J. Sæthre, K. J. Børve, J. J. Rehr, J. J. Kas, F. D. Vila, T. D. Thomas, and S. Svensson, Phys. Rev. Lett. **108**, 193005 (2012).
[10]N. Mårtensson, J. Söderström, S. Svensson, O. Travnikova, M. Patanen, C. Miron, L. J. Sæthre, K. J. Børve, T. D. Thomas, J. J. Kas, F. D. Vila, and J. J. Rehr, J. Phys.: Conf. Ser. **430**, 012131 (2013).
[11]E. Rühl, C. Heinzel, A. P. Hitchcock, and H. Baumgärtel, J. Chem. Phys. **98**, 2653 (1993).
[12]E. Rühl, C. Heinzel, A. P. Hitchcock, H. Schmelz, C. Reynaud, H. Baumgärtel, W. Drube, and R. Frahm, J. Chem. Phys. **98**, 6820 (1993).
[13]O. Björneholm, F. Federmann, F. Fossing, and T. Möller, Phys. Rev. Lett. **74**, 3017 (1995).
[14]H. Zhang, D. Rolles, Z. D. Pesic, J. D. Bozek, and N. Berrah, Phys. Rev. A **78**, 063201 (2008).
[15]M. Gisselbrecht, A. Lindgren, M. Tchaplyguine, F. Burmeister, G. Öhrwall, M. Lundwall, M. Lundin, R. R. Marinho, A. Naves de Brito, S. Svensson, O. Björneholm, and S. L. Sorensen, J. Chem. Phys. **123**, 194301 (2005).
[16]I. L. Bradeanu, R. Flesch, M. Meyer, H.-W. Jochims, and E. Rühl, Eur. Phys. J. D **36**, 173 (2005).
[17]M. Lundwall, A. Lindblad, G. Öhrwall, S. Svensson, and O. Björneholm, Phys. Rev. A **78**, 065201 (2008).
[18]O. Travnikova, J.-C. Liu, A. Lindblad, C. Nicolas, J. Söderström, V. Kimberg, F. Gelmukhanov, and C. Miron, Phys. Rev. Lett. **105**, 233001 (2010).
[19]V. Kimberg, A. Lindblad, J. Söderström, O. Travnikova, C. Nicolas, Y. P. Sun, F. Gelmukhanov, N. Kosugi, and C. Miron, Phys. Rev. X **3**, 011017 (2013).
[20]G. Öhrwall, M. Tchaplyguine, M. Gisselbrecht, M. Lundwall, R. Feifel, T. Rander, J. Schulz, R. R. T. Marinho, A. Lindgren, S. L. Sorensen, S. Svensson, and O. Björneholm, J. Phys. B: At., Mol. Opt. Phys. **36**, 3937 (2003).
[21]A. Lindblad, J. Söderström, C. Nicolas, E. Robert, and C. Miron, Rev. Sci. Instrum. **84**, 113105 (2013).
[22]O. F. Hagena, Z. Phys. D **4**, 291 (1987).
[23]U. Buck and R. Krohne, J. Chem. Phys. **105**, 5408 (1996).
[24]R. Karnbach, M. Joppien, J. Stapelfeldt, J. Wörmer, and T. Möller, Rev. Sci. Instrum. **64**, 2838 (1993).
[25]H. Bergersen, M. Abu-samha, J. Harnes, O. Björneholm, S. Svensson, L. J. Sæthre, and K. J. Børve, Phys. Chem. Chem. Phys. **8**, 1891 (2006).
[26]J. Söderlund, L. B. Kiss, G. A. Niklasson, and C. G. Granqvist, Phys. Rev. Lett. **80**, 2386 (1998).

[27]C.-R. Wang, R.-B. Huang, Z.-Y. Liu, and L.-S. Zheng, Chem. Phys. Lett. **227**, 103 (1994).
[28]J. Jauhiainen, A. Ausmees, A. Kivimäki, S. Osborne, A. N. de Brito, S. Aksela, S. Svensson, and H. Aksela, J. Electron Spectrosc. Relat. Phenom. **69**, 181 (1994).
[29]C. Nicolas and C. Miron, J. Electron Spectrosc. Relat. Phenom. **185**, 267 (2012).
[30]E. Kukk, SPANCF, Spectral Analysis by Curve Fitting Macro Package.
[31]E. Kukk, G. Snell, J. D. Bozek, W.-T. Cheng, and N. Berrah, Phys. Rev. A **63**, 062702 (2001).
[32]E. Kukk, K. Ueda, U. Hergenhahn, X.-J. Liu, G. Prümper, H. Yoshida, Y. Tamenori, C. Makochekanwa, T. Tanaka, M. Kitajima, and H. Tanaka, Phys. Rev. Lett. **95**, 133001 (2005).
[33]P. van der Straten, R. Morgenstern, and A. Niehaus, Z. Phys. D **8**, 35 (1988).
[34]B. Ravel and M. Newville, J. Synchrotron Radiat. **12**, 537 (2005).
[35]J. J. Rehr, J. J. Kas, M. P. Prange, A. P. Sorini, Y. Takimoto, and F. Vila, C. R. Phys. **10**, 548 (2009).
[36]K. Hermann, *Appendix E: Parameter Tables of Crystals* (Wiley-VCH Verlag GmbH & Co. KGaA, 2011), pp. 265–266.
[37]F. Calvo, J. P. K. Doye, and D. J. Wales, J. Chem. Phys. **114**, 7312 (2001).
[38]M. P. Seah and W. A. Dench, Surf. Interface Anal. **1**, 2 (1979).
[39]J. Yeh and I. Lindau, At. Data Nucl. Data Tables **32**, 1 (1985).
[40]J. Farges, M. F. de Feraudy, B. Raoult, and G. Torchet, J. Chem. Phys. **84**, 3491 (1986).
[41]N. V. Krainyukova, R. E. Boltnev, E. P. Bernard, V. V. Khmelenko, D. M. Lee, and V. Kiryukhin, Phys. Rev. Lett. **109**, 245505 (2012).
[42]QUASES-IMFP-TPP2M software, S. Tougaard, Quases-Tougaard Inc., 2000.
[43]S. Tanuma, C. J. Powell, and D. R. Penn, Surf. Interface Anal. **21**, 165 (1994).
[44]See supplementary material at http://dx.doi.org/10.1063/1.4931644 for details of the simulations.
[45]M. Tchaplyguine, R. R. Marinho, M. Gisselbrecht, J. Schulz, N. Mårtensson, S. L. Sorensen, A. Naves de Brito, R. Feifel, G. Öhrwall, M. Lundwall, S. Svensson, and O. Björneholm, J. Chem. Phys. **120**, 345 (2004).
[46]W. J. Huang, R. Sun, J. Tao, L. D. Menard, R. G. Nuzzo, and J. M. Luo, Nat. Mater. **7**, 308 (2008).